Ab Initio Transition State Searching in Complex Systems: Fatty Acid Decarboxylation in Minerals

ARTICLE *in* THE JOURNAL OF PHYSICAL CHEMISTRY A · MARCH 2011

Impact Factor: 2.69 · DOI: 10.1021/jp200106x · Source: PubMed

3 AUTHORS, INCLUDING:

Dawn Lesley Geatches
Stanford University
11 PUBLICATIONS **42** CITATIONS
SEE PROFILE

Chris Greenwell
Durham University
59 PUBLICATIONS **1,562** CITATIONS
SEE PROFILE

THE JOURNAL OF PHYSICAL CHEMISTRY A

ARTICLE

pubs.acs.org/JPCA

Ab Initio Transition State Searching in Complex Systems: Fatty Acid Decarboxylation in Minerals.

Dawn L. Geatches,*[,†] H. Christopher Greenwell,[‡,§] and Stewart J. Clark[†]

[†]Physics Department and [‡]Earth Sciences Department, Durham University, South Road, Durham, DH1 3LE, United Kingdom

ABSTRACT: Because of the importance of mineral catalyzed decarboxylation reactions in both crude oil formation and, increasingly, biofuel production, we present a model study into the decarboxylation of the shortest fatty acid, propionic acid C_2H_5COOH, into an alkane and CO_2 catalyzed by a pyrophillite-like, phyllosilicate clay. To identify the decarboxylation pathway, we searched for a transition state between the reactant, comprised of the clay plus interlayer fatty acid, and the product, comprised of the clay plus interlayer alkane and carbon dioxide. Using linear and quadratic synchronous transit mechanisms we searched for a transition state followed by vibrational analysis to verify the intermediate found as a transition state. We employed a periodic cell, planewave, ab initio density functional theory computation to examine total energy differences, Mulliken charges, vibrational frequencies, and the frontier orbitals of the reactants, intermediates, and products. The results show that interpretation of vibrational data, Mulliken charges and Fermi-level orbital occupancies is necessary for the classification of a transition state in this type of mixed bulk surface plus interlayer species, clay-organic system.

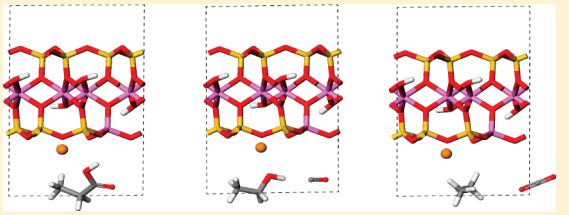

1. INTRODUCTION

Clay minerals have played an important role in the development of Western society from the production of bricks, tiles, and pottery to drug delivery agents, catalysts[1] and pet litter. The wide-ranging use of clays is due to their molecular properties (e.g., molecular sieve catalysts[2]) and phyllosilicate structure (e.g., adsorbents) where sheets of aluminosilicate of octahedral (Al) and tetrahedral (Si) coordination are interleaved. These clays have octahedral sheets whose general form is $Al_4O_8(OH)_4$ and tetrahedral sheets of Si_4O_6. Isomorphic substitution often occurs in both the octahedral and tetrahedral sheets[3] with an ion such as Mg^{2+} for Al^{3+} in the octahedral sheet and Al^{3+} for Si^{4+} in the tetrahedral sheet. The net negative charge caused by the substitutions is balanced by the presence of exchangeable cations, for example Na^+ or Ca^{2+} between the clay layers.

The presence of catalytic sites within clays is important in the formation of fossil oil where a fatty acid of biological origin, has been trapped within the interlayers of the clay and through a process of burial diagenesis becomes decarboxylated to an alkane and carbon dioxide. Decarboxylation describes the removal of CO_2 from a carboxylic acid, a reaction that is widely studied in organic chemistry, biochemistry, and geochemistry. Such a decarboxylation pathway within phyllosilicate clays was theorized by Almon and Johns[4] in 1975 from a series of experiments using various clay minerals including pyrophyllite. Their experimental results lead to Almon and Johns hypothesizing a decarboxylation pathway involving a free radical intermediate.

The investigation we present here is a continuation from our previous study[5] that was itself based on the 1975 Almon and Johns paper.[4] In that study, we used density functional theory (DFT) to determine the optimal modeling system for a decarboxylation reaction catalyzed within a pyrophillite-like phyllosilicate involving a short chain fatty acid, propionic acid (reactant), and ethane plus carbon dioxide (product). The aim of the present study is to locate an intermediate between the reactant and product identified in our earlier work and verify it as a transition state using vibrational analysis.

Transition states are short-lived intermediates between reactants and products; they are found at a stationary point on a chemical reaction pathway and describe the activation energy of a chemical reaction and the relative stability of the product. Their location is important in identifying the pathway of a chemical reaction, such as in research into enzymes[6,7] and the production of enzyme inhibitors[8] to calculating reliable rate coefficients.[9] Transition states can be located by various means such as eigenvector following,[10] nudged elastic band,[11] string method,[12] and statistical transition path sampling,[13] although for large systems there is no obvious way to predict the efficiency of one method over another.[14] In this investigation, we use linear and quadratic synchronous transition state (LST/QST) searches,[15] similar to a practiced method that involves the identification of intermediates (see ref 16 for more details), although that particular method relies on chemical intuition or a priori knowledge of the reaction pathway and does not need the reactant and product configurations. In contrast, LST/QST uses the reactant and product geometries and assumes nothing about the decarboxylation reaction pathway, hence it could be described as an ab initio transition state search.

An examination of the current literature shows that DFT and the B3LYP functional have been used to study the kinetics of decarboxylation[16] and to identify transition states by vibrational analysis.[17,18] These and other DFT investigations have mostly been

Received: January 5, 2011
Revised: February 1, 2011
Published: March 04, 2011

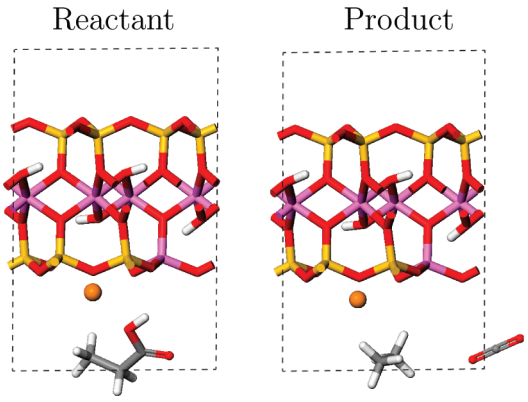

Figure 1. A single unit cell of pyrophillite (with an aluminum substitution in the tetrahedral layer) and guest molecule of one of the simpler model fatty acids, propionic acid within the interlayer space of the reactant model and ethane plus carbon dioxide in the product model. See Table 1 for initial geometry optimized dimensions. Oxygen, red; hydrogen, white; aluminum, pink; carbon, gray; silicon, yellow; sodium, orange. The dashed line is the periodic boundary of a unit cell. All subsequent figures use the same color scheme.

carried out on cluster models[1] and isolated molecules in the gas phase;[19] this contrasts with our study where we use periodic models to represent an extended clay surface. As well as investigating decarboxylation, DFT has been used extensively to determine the structure of clays[20] and their vibrational properties[21,22] and structural defects[23] as well as examining the catalytic activity of anionic clays.[24]

In this study, we have brought together several facets of the above in a way that we believe is uncommon if not unique. We use linear response density functional perturbation theory (DFPT) to calculate the vibrational frequencies of a periodic clay system containing a gas phaselike molecule in the interlayer space, to identify an intermediate of a decarboxylation reaction and verify it as a transition state with the aim of gaining insight into the chemical pathway of clay-catalyzed decarboxylation.

The location of a transition state would ultimately help identify the chemical pathway of this form of fossil oil production. This is of particular relevance today as the fatty acids in biofuel crops are of a similar type to those modeled in this reaction,[25,26] hence the investigation of this reaction and the insight gained into the catalytic conversion of fatty acids into high-grade fuel offers the potential to contribute to the efficient production of biofuels.

The remainder of this paper is divided into a Method section describing the transition state search and the verification of an intermediate as a transition state using lattice dynamics computations. This is followed by the Results and Discussion section detailing the vibrational analysis, Mulliken charges, and Kohn−Sham orbitals; finally, the study is summarized in the Conclusion.

2. METHOD

2.1. Structures. Pyrophillite is a 2:1, dioctahedral, uncharged, aluminosilicate clay. A unit cell of charged, pyrophillite-like aluminosilicate $Al_5Si_7O_{20}(OH)_4$, (henceforth called pyrophillite), space group $P\bar{1}$ was constructed as detailed in ref 5. The reactant model is comprised of a unit cell of pyrophillite plus propionic acid and the product model a unit cell of pyrophillite plus the alkane C_2H_6 and CO_2 as shown in Figure 1; the cell dimensions are shown in Table 1. From this point onward we use the term

Table 1. Lattice Parameters of a Unit Cell of Pyrophillite after Geometry Optimization[a]

DFT (PBE)[5]		experiment[27]		other DFT (PB86[b])[28]	
a = 5.22	α = 90.87	a = 5.18	α = 90.00	a = 5.119	α = 90.77
b = 9.07	β = 100.00	b = 8.96	β = 99.9	b = 8.911	β = 100.96
c = 9.73	γ = 89.65	c = 9.97	γ = 90.0	c = 9.065	γ = 89.91

[a] The first column reproduces the results from our previous paper with no interlayer molecules; the c-length in our previous study converged to 14.5 Å on the inclusion of a molecule of propionic acid, hence the same extension was used in this study. Lengths are in angstroms and angles in degrees. [b] A semiempirical functional with a fitted parameter for the exchange part.

"reactant" and "product" respectively to describe these models. The optimal reactant and product models were found to incorporate an aluminum substitution in the tetrahedral sheet, which is thought to be the site of catalytic activity[4] plus a sodium atom that counterbalances the charge generated by this and enables electron transfer between the guest organic molecule and the clay. These reactant and product models provided the end points for the transition state search detailed in the following section.

2.2. Computational Details. We employed the CASTEP code[29] with a planewave basis set within the DFT formalism.[30,31] Convergence testing from our previous study showed that a planewave basis represented by a kinetic energy cutoff of 550 eV using a coarse grid of 1.75 gave an energy difference in total energies of less than 0.04 eV per unit cell for higher cut-offs and the Brillouin zone integrations were optimal using a grid containing two k-points to converge the calculation at a volume appropriate for these simulations.[5]

We used the generalized gradient approximation (GGA) density functional, specifically Perdew, Burke, and Ernzerhof (PBE)[32] as this describes molecular bonding to a greater accuracy than does the local density approximation (LDA).[33] PBE ultrasoft pseudopotentials[34] were used that are consistent with the PBE exchange functional. The (geometry) optimizer was Broyden−Fletcher−Goldfarb−Shanno (BFGS) and the electronic method was ensemble density functional theory (EDFT).[35] As a transition state search as implemented in CASTEP requires force tolerance criteria of less than 0.1 eV/Å, we relaxed the geometries of the reactant and product models to the following criteria: electronic energy tolerance: 10^{-10} eV; geometry optimization−energy change per ion: 10^{-8} eV; maximum force: 0.025 eV/Å; change in distance: 0.0005 Å. All calculations were carried out without spin polarization.

Our transition state search calculations used an initial linear synchronous transit search method to identify the upper bound on a transition state that is determined only by the geometry of the reactant, intermediate and product (see ref 36 for further details). This was followed by a quadratic synchronous transit search that refines this initial intermediate toward a transition state using conjugate gradient refinement.

An intermediate configuration was found, shown in Figure 2, that displayed an interlayer species different in configuration to both that of the reactant and product implying it was a possible transition state. To determine whether it was a transition state we carried out a lattice dynamics calculation, as described in the next section.

2.2.1. Lattice Dynamics. The energy landscape of a transition state is a saddle point, such that there is an increase in energy in traversing the saddle in all directions but one, and a decrease in

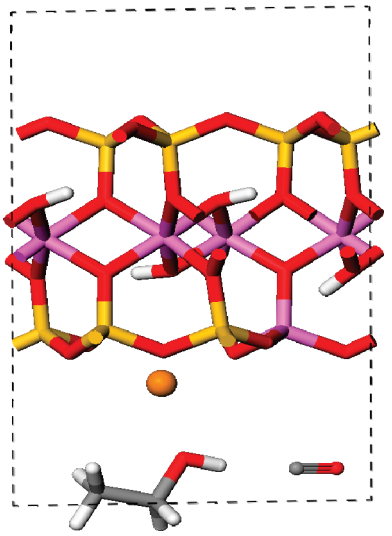

Figure 2. Intermediate state following the geometry optimization of the maximum of a quadratic synchronous transition search.

the other. The mathematical description of this is a single imaginary eigenfrequency identifying the direction of decreasing energy. It is possible to detect this vibrational mode and hence verify a transition state using lattice dynamics calculations.

The linear response calculation, density functional perturbation theory (DFPT[37]), implemented in CASTEP computes the lattice dynamic responses of a bulk material for a range of electromagnetic frequencies (q-values/points). DFPT is currently implemented for norm-conserving pseudopotentials.[38] A complete relaxation of the lattice parameters and the atomic positions of the reactant, intermediate, and product models within the ultrasoft pseudopotential approximation required hundreds of hours of computational time; thus we made a decision to keep the lattice parameters fixed in subsequent calculations involving norm-conserving pseudopotentials with one exception: a clay-only model. Consequently, keeping the lattice parameters fixed, we allowed only the atoms to relax and reoptimized the reactant, intermediate, and product models with the norm-conserving pseudopotentials; two clay-only models were also optimized, one with lattice parameters and atomic positions relaxed and one with relaxation of the atomic positions only. We used a coarse grid scale of 2.0, 550 eV, two k-points and the convergence criteria previously stated in Section 2.2, paragraph two. An energy-differences convergence test showed that for a coarse grid of 2.0 550 eV produced energy convergence to 1 meV. The additional convergence criteria used for the linear response calculation were as follows: phonon energy tolerance: 10^{-5}eV; phonon convergence tolerance: 10^{-5}eV/Å^2; phonon preconditioner: Teter, Payne, and Allan (TPA[39]).

DFPT calculations were carried out on the optimized geometry of the intermediate at the gamma point, $q = 0$ followed by a dispersion curve based on a coarse, reciprocal space, Monkhurst Pack grid of q-points, [10, 5, 1], with an interpolation of q-point spacing of 0.01. This spacing was found to be optimal as spacing less than this produced no further refinement in the results. This was repeated for the reactant, product, and the clay-only model plus the full relaxation of the clay-only model including its lattice parameters. The latter two cases involved solely the clay surface without any guest molecules.

Table 2. Energy Differences (Δ_{A-B}) of the Optimized Models Using Ultrasoft and Norm-Conserving Pseudopotentials Where R Is Reactant, I Is Intermediate, and P Is Product

	energy difference (eV)	
	ultrasoft	norm-conserving
Δ_{I-R}	1.2026	0.8773
Δ_{I-P}	1.3413	1.6467
Δ_{P-R}	−0.1387	−0.7694

$$H_{2n+1}C_n - COOH \xrightarrow{[+2H_2 - H_2O]} H_{2n+3}C_{n+1} - OH \xrightarrow{[-H_2O]} C_{n+1}H_{2n+2}$$

Figure 3. Hydrodeoxygenation reaction scheme of a fatty acid.[41]

3. RESULTS AND DISCUSSION

3.1. Finding the Transition State. The LST/QST searches produced a configuration of interlayer species, consistent with a possible transition state between the reactant and product, see Figure 2. The energy differences are shown in Table 2. This intermediate is ethanol CH_3CH_2OH plus CO, which are not intermediates hypothesized by Almon and Johns as they deduced an organic free radical intermediate or, in the absence of water, the involvement of a carbonium ion.[4]

An examination of the energy differences between the intermediate, reactant, and product, Table 2, shows that in both pseudopotential approximations there is a positive energy difference between the intermediate and the reactant and the intermediate and the product due to the higher energy of the intermediate, which is consistent with the characteristics of a transition state between a reactant and product. Although the two approximations show a difference in magnitude of the energy differences between the reactant, product, and intermediate, we found these results acceptable within the scope of this study, as we did not expect to obtain quantitative data about reaction rates from these simulations.

Much of the initial interest in mineral-mediated decarboxylation reactions arose from issues surrounding the formation of crude oil and its extraction and purification. Early work by Almon and Johns evidenced that one possible pathway for decarboxylation under putative reservoir conditions involved free radical mechanisms with increased conversion of fatty acids in the presence of radical promoters and, conversely, a decrease in reactivity in the presence of free radical inhibitors. In other work by Zhang et al., who used metal oxide catalysts to reduce the total acid number (caused by naphthenic acid) in crude oil, to increase the value of the product, cationic/anionic and concerted pathways were proposed as potential reaction mechanisms.[40] However, the transition state we found does not suggest a reaction pathway in agreement with any of the above mechanisms.

As previously stated, decarboxylation has become of interest through the desire to be able to produce fossil fuel-like products from plant oils, which are primarily composed of triacyl glycerides, based on fatty acid structures. In this present study, we have identified a physically relevant transition state in the form of an alcohol. This alcohol subsequently undergoes further reduction down to the hydrocarbon with the simultaneous formation of CO_2. Such reactions are not without precedent; dehydration/hydrogenation reactions of fatty acids and their esters have been shown to involve alcohol intermediates in studies of biofuel production[41] as illustrated in Figure 3.

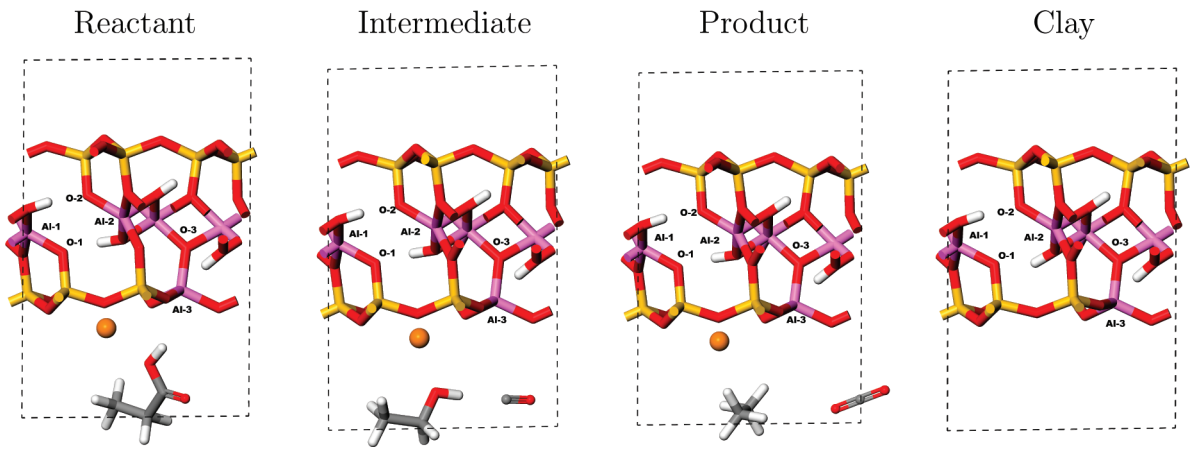

Figure 4. Geometry optimized models using the norm-conserving pseudopotentials. The labeled atoms are referred to in Tables 4 and 5.

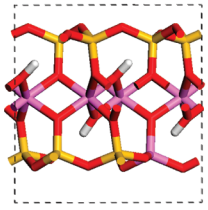

Lattice dimensions

$a = 4.97$ $\alpha = 90.09$
$b = 8.63$ $\beta = 100.88$
$c = 9.24$ $\gamma = 89.60$

Figure 5. Unit cell of the clay layer (without any interlayer species) after geometry optimization where the whole cell and contents have been allowed to relax within the norm-conserving pseudopotential approximation. Lengths are in angstroms and angles in degrees.

There are, however, several caveats to note. We use a reasonably simplistic model to probe the reaction mechanism and, owing to periodic boundary conditions, are essentially considering a unimolecular reactant state. Though we employ an ab initio approach, we define our expected products and if, as is highly likely in the case of free radical reactions, multiple transition states with small energy separations exist on that pathway, our method may not uncover them. An alternative approach within our methodological constraints would be to specify explicit intermediate states.

Additionally, it should be noted that the experimental reaction rates were rather slow with only 2% conversion to the alkane product even at elevated temperatures of 250 °C and that Almon and Johns did state that their proposed decarboxylation mechanism probably did not "reflect reality except in the broadest sense".[4]

Both their study and ours agree that a decarboxylation reaction within a clay environment involves the transfer of electrons to the clay minerals, which we show in subsequent sections. Furthermore, our transition state opens up the possibility in further future work to determine an intrinsic reaction coordinate (IRC) path[42] and to analyze the mechanics of a reaction[43] leading from the reactant to the product via this transition state and, possibly, many others.

3.2. Vibrational Analysis. On geometry optimization of the intermediate configuration using norm-conserving pseudopotentials and visualization of the resulting geometry, it was found that there was a distortion in the clay layer above the position of the sodium atom, see Figure 4. When repeating the optimization on the reactant, product and clay-only layer using norm-conserving pseudopotentials, the same distortion of the clay layer appeared. When we allowed the lattice and atomic positions of the clay-only layer to relax, there was no distortion in the clay layer, see Figure 5. This implies the distortion is a direct result of using the norm-conserving pseudopotentials without allowing the lattice parameters to relax. These lattice lengths are within 5% of those obtained using the ultrasoft pseudopotentials and although the clay layer has been distorted, a comparison of Figures 1, 2, and 4 shows that the configurations of the interlayer species appear similar in both pseudopotential approximations, probably by virtue of the vacuum of the interlayer enabling the organic molecules to relax without the imposed lattice restraint. The aim of this study is to identify a transition state configuration and, as both pseudopotential approximations have produced the same configuration when geometry optimized, this elicits the following question: how much has the distortion in the clay layer affected the verification of a transition state using vibrational analysis?

Table 3. Four Lowest Eigenvalues from the Phonon Calculation on Each Model Where "Y" and "N" Refer to Raman Activity "Yes" and "No", Respectively (Units Are in cm^{-1})

reactant		intermediate		product		clay	
$-0.02i$	N	$-45.35i$	Y	$-53.9i$	Y	$-0.02i$	N
$-0.02i$	N	$-0.02i$	N	$-0.03i$	N	$-0.02i$	N
$-0.02i$	N	$-0.02i$	N	$-0.02i$	N	$-0.02i$	N
38.22	Y	$-0.02i$	Y	$-0.02i$	N	55.66	Y

The four lowest eigenfrequencies of the phonon calculation (see Table 3) for the commensurate $q = 0$ point show that the intermediate has four imaginary frequencies, three of which are shared with the reactant and clay and two with the product. The three frequencies with the value $-0.02i$ cm^{-1} and $-0.03i$ cm^{-1} represent the three translational vibrations of the lattice in the x-, y- and z-directions. The difference between these values and zero is acceptable noise of the calculation in the context of a range of frequencies that extends to 3700 cm^{-1}, together with the force convergence criteria of the geometry optimization. The results for the reactant and clay models do not contain any large imaginary frequencies, implying that the imaginary frequencies found in the intermediate and product are not due to using the norm-conserving pseudopotentials and the imposed lattice constraint and the effect these have had on the clay.

dx.doi.org/10.1021/jp200106x |J. Phys. Chem. A 2011, 115, 2658–2667

The largest imaginary frequency of the intermediate is indicative of a transition state but, as can be seen in the results, the product also has a large imaginary eigenfrequency although the product was assumed to be stable. Visualization of these imaginary modes show for the intermediate an oscillation of the OH branch of ethanol toward CO suggesting that an application of energy will initiate a reaction between the two separate molecules of this intermediate stage, which would then form the product alkane and CO_2 and therefore this intermediate is a transition state. In contrast, visualization of the imaginary mode of the product model shows an oscillation of the alkane in the *z*-direction pivoted at one end with no feasible interaction with the local environment. As this imaginary vibrational mode does not indicate a change of configuration, it is not indicative of a transition state. See Figure 6 for a static visualization of these modes.

An analysis of other vibrational modes shows agreement with both experimental[44] and computational results:[28,45] O−H vibration mode at 930 cm^{-1}, Si−O modes at 1100 and 1104 cm^{-1}, and O−H stretching at 3644 and 3663 cm^{-1} involving the central-cell O−H. This indicates that the results concerning the imaginary vibrational modes have equal validity and that the distortion caused by the lattice constraint has had a minimal effect on vibrational frequencies.

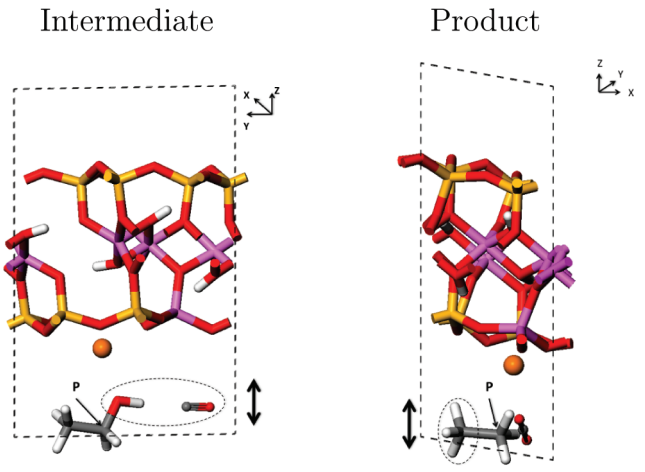

Figure 6. A schematic of the imaginary vibrational modes of the intermediate and the product. The area encircled by the dashed line indicates the atoms involved in the vibration. The double-headed arrow indicates the direction of vibration and the point labeled P represents the intersection of the pivotal axis with the organic molecule. In the intermediate, this is the *x*-axis and in the product, this is the *z*-axis.

Table 4. Distances between the Al's Marked on Figure 4[a]

	Al1to Al2 (Å)	
model	ultrasoft	norm-conserving
reactant	3.066	3.925
intermediate	3.070	3.926
product	3.070	3.919
clay layer-1		3.993
clay layer-2		2.877

[a] Clay layer-1 refers to the clay only layer without lattice relaxation and clay layer-2 to the clay only layer with lattice relaxation.

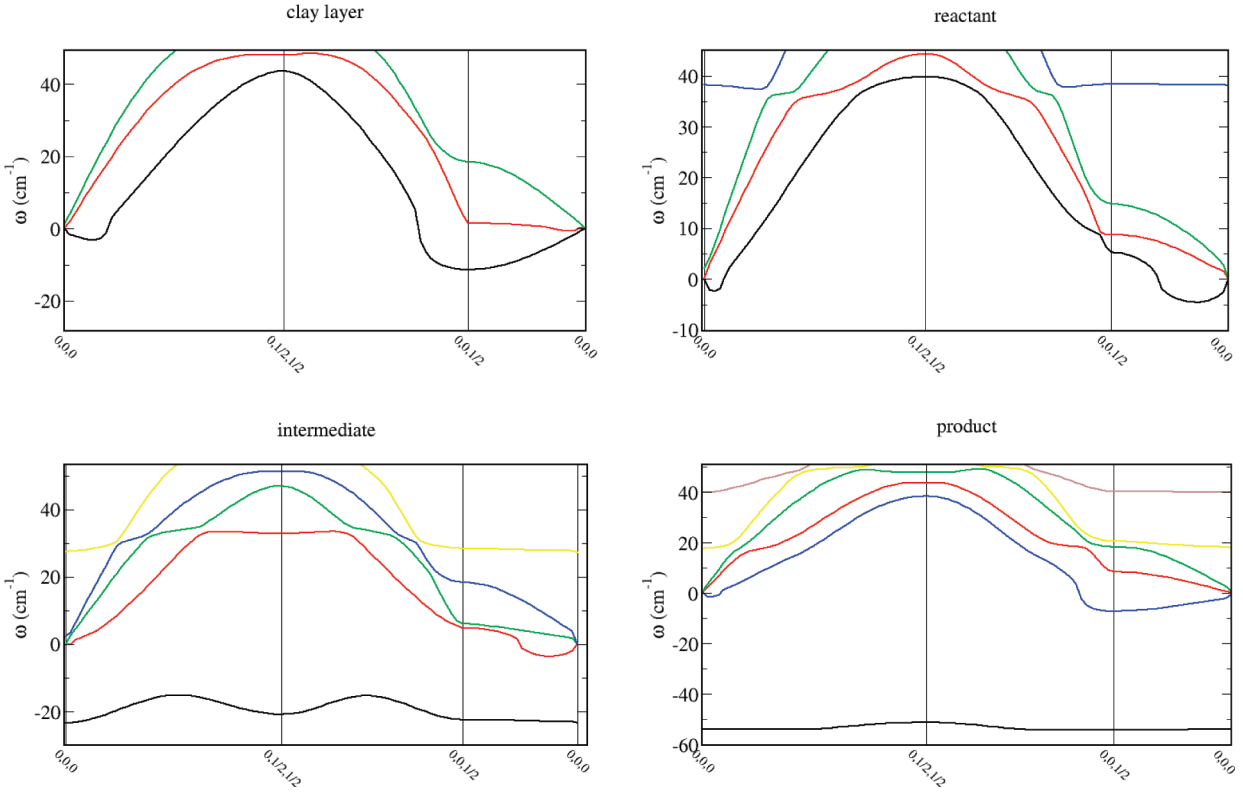

Figure 7. Dispersion curves from lattice dynamics calculations on a fine grid for a short path through the Brillouin zone. The negative part of the *y*-axis represents imaginary frequencies.

dx.doi.org/10.1021/jp200106x |*J. Phys. Chem. A* 2011, 115, 2658–2667

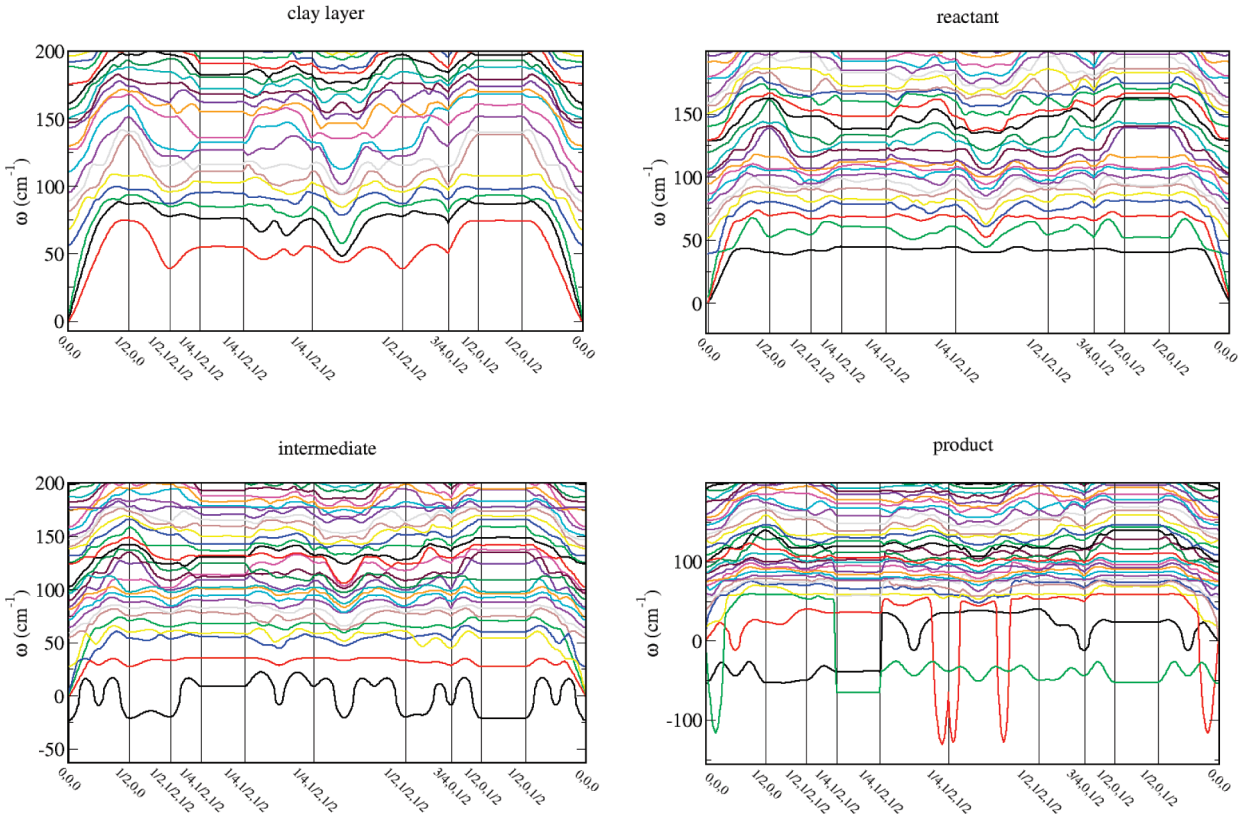

Figure 8. Dispersion curves from lattice dynamics calculations on a fine grid for a long path through the Brillouin zone. The negative part of the *y*-axis represents imaginary frequencies.

Table 5. Mulliken Charges of the Atoms Marked on Figure *4* within the Two Pseudopotential Approximations Where R is Reactant, I is Intermediate, P is Product, C-1 Refers to the Clay Only Layer without Lattice Relaxation, and C-2 to the Clay Only Layer with Lattice Relaxation

	Ultrasofts				Norm-conserving				Ultrasofts			Norm-conserving		
model	Al1	Al2	Al3	Na	Al1	Al2	Al3	Na	O1	O2	O3	O1	O2	O3
R	1.79	1.77	1.88	1.41	1.89	1.89	1.87	1.45	−1.12	−1.14	−1.18	−1.18	−1.19	−1.19
I	1.79	1.78	1.88	1.27	1.89	1.89	1.86	1.39	−1.12	−1.14	−1.18	−1.18	−1.19	−1.20
P	1.79	1.78	1.88	1.45	1.89	1.89	1.86	1.56	−1.12	−1.14	−1.18	−1.18	−1.20	−1.20
C-1					1.92	1.93	2.02					−1.13	−1.15	−1.16
C-2					1.87	1.88	1.98					−1.15	−1.15	−1.09

Table 4 shows the effect of using norm-conserving pseudopotentials on the bond distances between the aluminums and the dispersion curves for all four models are shown in Figure 7. All four dispersion curves show a negative dip between *k*-points [0,0,0] and [0,0,0.5]. The common configuration between these four models is the clay layer that suggests the negative (i.e., imaginary) dip in the dispersion curves is a result of the instability in the clay layer created as an artifact of using norm-conserving pseudopotentials and keeping the lattice parameters fixed. The lattice was not reoptimized at the same time as the contents because we had an optimized cell that agreed with previous DFT calculations and experimental results (see Table 1) and were therefore confident that any intermediate found in a transition state search using these optimized models would likewise accurately reflect experimental geometries. Although a distortion was created in the clay layer, the relative configurations of the interlayer guests remained the same on the pseudopotential substitution, hence the change caused by the substitution did not detract from the main aim of this study.

Figure 8 shows the dispersion curves for a longer path through the Brillouin zone, which does not include any section of the path that produces the dispersion curves shown in Figure 7. The longer-path dispersion curves add further evidence to the intermediate being a transition state, as within this model there is only one path displaying imaginary frequencies, whereas in the product model there are three and in the clay-only and reactant models there are none. The three paths of the product model displaying imaginary frequencies indicate an instability in the system along this path, unique to the product model. Therefore, the conclusion from this analysis suggests that the intermediate has been correctly identified as a transition state and the product model contains a system instability.

dx.doi.org/10.1021/jp200106x |*J. Phys. Chem. A* 2011, 115, 2658–2667

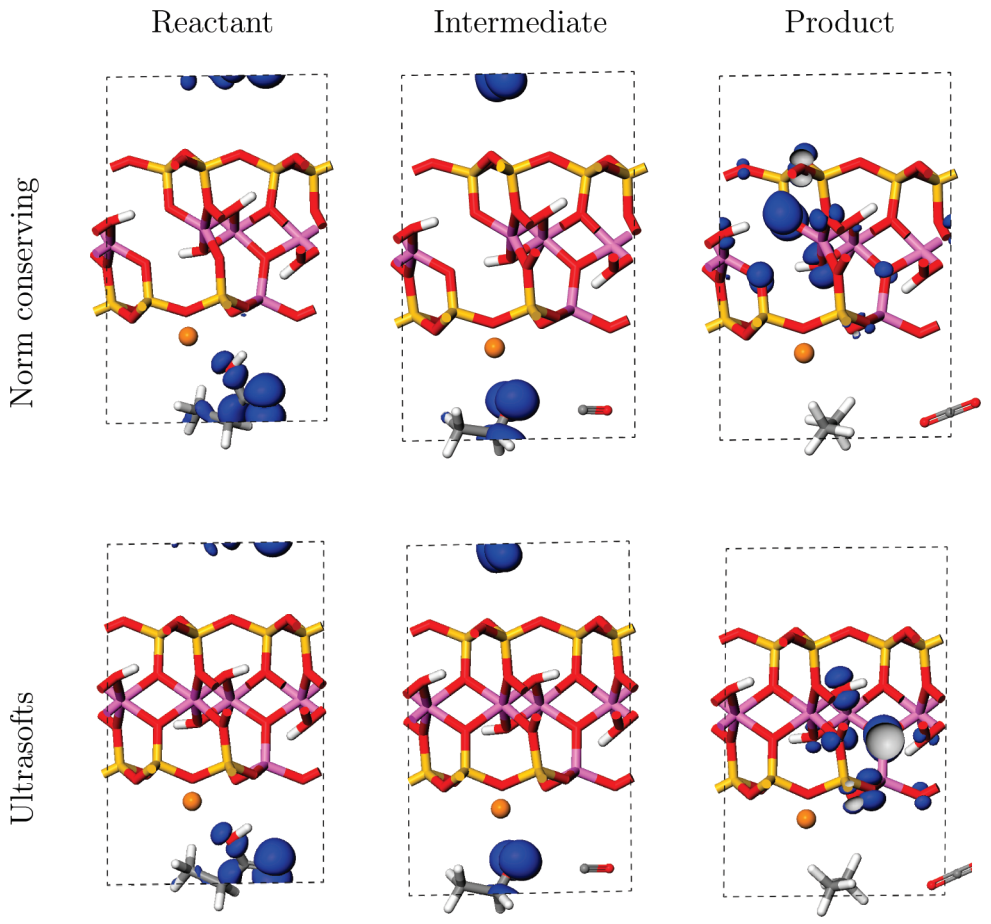

Figure 9. Fermi-level orbitals shown in blue where the upper row models use the norm-conserving pseudopotentials and the lower row the ultrasofts.

3.3. Mulliken Charges and Kohn−Sham Orbitals. The Mulliken charges of the aluminums and oxygens labeled in Figure 4 within the clay layers (see Table 5) show that in the norm-conserving pseudopotential calculations Al1 and Al2 are allocated a higher charge than in the ultrasoft calculations whereas Al3 is between 1.86 and 1.88 for both approximations for the reactant, intermediate, and product. This shows that the tetrahedral sheet aluminum (Al3) has the same charge as the octahedral sheet aluminums when the lattice has not been allowed to relax, however, when it is able to relax (model C-2) the tetrahedral sheet aluminum has a charge higher than Al1 and Al2 by 0.1e which is the same as the difference between these aluminums within the ultrasoft approximation. The same trend in the clay-only layers, C-1 and C-2, where sodium is absent is seen in both scenarios which implies that despite the lattice restraint the absence of sodium results in a higher charge on Al3 due to the decrease in electron density. Therefore, the lattice restraint has had no effect on the mechanism of electron donation to the clay layer.

An examination of the charges on the oxygens shows that within the norm-conserving pseudopotential approximation, they range from −1.18 to −1.20e for the reactant, intermediate, and product models whereas within the ultrasoft approximation they range from −1.12 to −1.18e. When the clay-only layer is allowed to relax (C-2), the charges on the oxygens within the octahedral sheet both become −1.15e and the oxygen closest to the tetrahedral aluminum becomes −1.09e. This less negative charge compared to that of O3 in the reactant (−1.1e), intermediate (−1.20e), and product (−1.20e) models appears to be due to the absence of sodium and no electron donation and hence the consequent reduction in electron density. The clay-only layer that was not allowed to relax (C-1) shows a charge of −1.16e on O3 even in the absence of sodium and could have assumed some of the negative charge from O1 which has a charge of −1.13e. The charges on the sodium within both pseudopotential approximations show different values but the same trend: a decrease from the reactant to intermediate then an increase to the product. The higher charges of the oxygens for C-1 and C-2 in the norm-conserving models than those of the oxygens in both pseudopotential approximations for the reactant, intermediate, and product models add further evidence to the assertion that sodium is the source of electron donation.

These Mulliken charges show that the two approximations have resulted in different charge distributions within the clay layers which suggests that where Fermi level orbitals exist within this layer, their distribution may differ depending on the pseudopotential approximation. This is indeed the case in the product model (see Figure 9) where there is clay layer involvement of the Fermi level orbitals. The two pseudopotential approximations display different Fermi level orbital distributions particularly around the aluminum and oxygen atoms discussed above. However, to what extent have the Mulliken charges and the Fermi level orbitals of the interlayer species been affected by the clay layer distortion?

The Mulliken charges[46] of the reactant atoms (Figure 10) show that it has been allocated a relative charge of −0.31e and −0.30e in

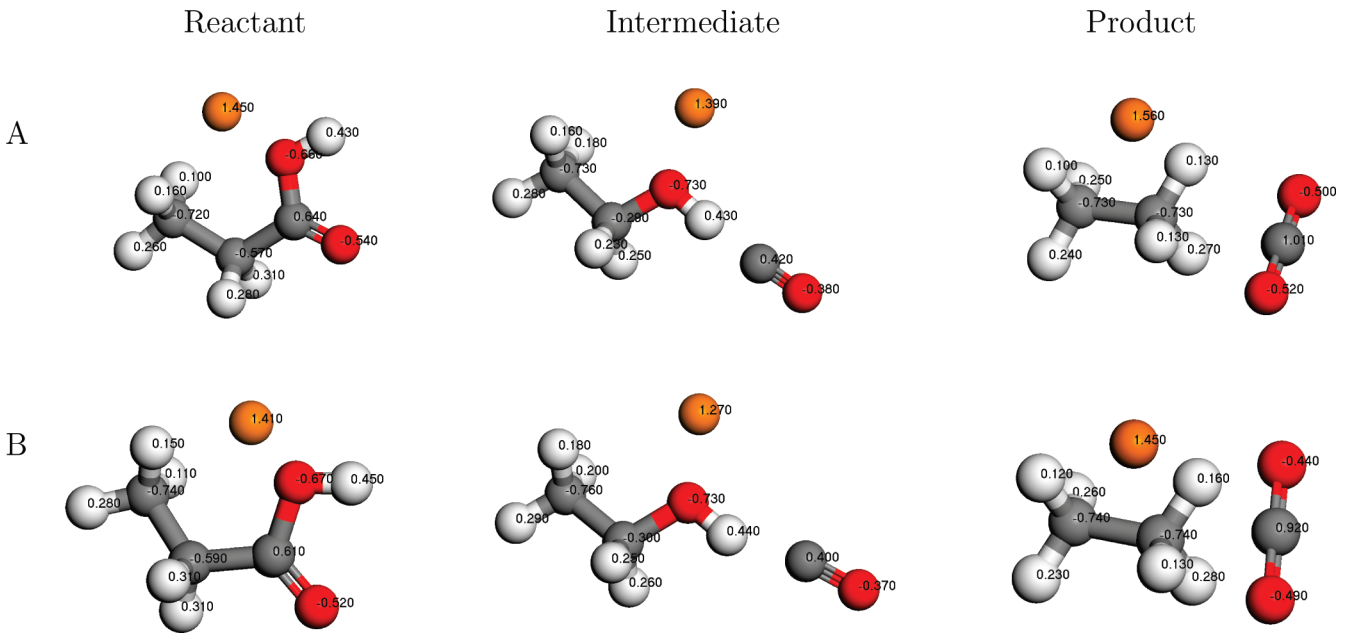

Figure 10. Mulliken charges on the interlayer species where set A is with norm-conserving pseudopotentials and B with ultrasofts. For display purposes, the relative positions of the molecules to each other are scaled; see Figure 4 for the accurate representation of relative geometries.

the norm-conserving and ultrasoft approximations. An examination of the highest occupied molecular orbitals (HOMO) or Fermi level orbitals (Figure 9) shows that the electrons most likely to react are those on the fatty acid in both pseudopotential cases.

The Mulliken charges on the ethanol of the intermediate model give its overall relative charge of −0.22e and −0.17e in the norm-conserving and ultrasoft approximations. A closer examination of the charges of the oxygen and hydrogen atoms of the hydroxyl bond shows a difference of 0.01e between the two approximations and the Fermi-level orbitals in both cases are situated on the ethanol, including this bond. This is consistent with the analysis of the imaginary vibrational mode that showed a joint vibration between the hydroxyl bond of the ethanol and the carbon monoxide and hence the supposition that an application of energy would most probably cause the Fermi level electrons to react, decreasing the overall energy of the system by interacting with CO to form the product.

The overall Mulliken charge on the alkane in the product model is −0.34e and −0.30e in the norm-conserving and ultrasoft approximations. This larger negative charge on the alkane in the norm-conserving approximation together with the positive charge of 1.56e on the sodium could be creating a dipole. The difference in Mulliken charge between the sodium and alkane is greatest in this model, hence the creation of a $z-$ direction oscillation as discussed previously and represented in the lattice dynamics calculation by the imaginary eigenfrequency given in Table 3. The Fermi-level orbitals in both approximations show dissipation within the clay layer only, but differ in their distributions as commented on in the previous paragraphs.

Thus it can be said that the imaginary frequency of the alkane model is a secondary effect of using norm-conserving pseudopotentials without allowing relaxation of the lattice, further supporting our earlier assertion that there has been no direct effect on the interlayer configurations themselves and hence the intermediate species has been correctly identified and verified as a transition state.

4. CONCLUSION

Conceptually, low-order layered organo-mineral structures are among the most difficult to accurately characterize with only limited information available from analytical methods. As such, computer simulation has become an essential adjunct to experiment to characterize the structure of such systems fully.[3,47] The situation is even more challenging if reaction mechanisms are to be studied; the sheer complexity of a mineral matrix, organic material, water, and applied external conditions make the study of reaction mechanisms in such systems inherently difficult. In this paper, we present advances in the application of computational methods to address this challenge.

Here, for the first time, we present ab initio transition state search algorithms with DFT methods to probe potential reaction pathways in decarboxylation reactions in smectite clay minerals. Such reactions are believed to be responsible for crude oil formation under reservoir conditions[4] and are increasingly of interest in biomass−biofuel conversions.[48]

Clearly, to be able to address this topic on a meaningful computational time scale a number of constraints must be imposed on our model system. We elected to use fixed atomic composition, remove interlayer water, and in this study have no Fe substitutions in our model (likely to be important in radical processes). Furthermore, we remove the effects of external temperature and pressure.

Within our elected level of description, we have identified a physically relevant transition state in the form of an alcohol intermediate, which subsequently undergoes further reduction down to the hydrocarbon with the formation of CO_2. Such reactions are not without precedent, dehydration/hydrogenation reactions of fatty acids and their esters have been shown to involve alcohol intermediates in studies of biofuel production.[41]

In summary, our studies are evolving to capture the fundamental elements of catalysis in complex mineral systems. Through using an ab initio approach we do not impose a priori conditions or assumptions upon our system of interest. Through

our chosen DFT methodology, we also obtain information regarding the electronic structure of the system at critical stages along the reaction coordinate and hence can readily calculate spectroscopic data, which may aid in the interpretation of experimental analytical data.

Such an approach presents a powerful tool to elucidate reaction mechanisms in complex systems and we proceed in future work to identify the role of other parameters such as the presence of Fe substitutions, more than one reactant molecule, and interlayer water.

AUTHOR INFORMATION

Corresponding Author

*Tel: +44 (0)191 3343549. E-mail: d.l.geatches@dur.ac.uk.

Present Addresses

[§]Laboratoire de Chimie Physique et Microbiologie pour L'Environnement (LCPME), UMR-7564 CNRS-UHP Nancy Universite′, 405 rue de Vandoeuvre, 54600 Villers-les-Nancy, France.

ACKNOWLEDGMENT

This work made use of the facilities of HECToR, the U.K.'s national high-performance computing service, which is provided by UoE HPCx Ltd. at the University of Edinburgh, Cray Inc., and NAG Ltd. and funded by the Office of Science and Technology through EPSRC's High End Computing Programme. Thanks also to the EPSRC for funding D.L.G.

REFERENCES

(1) Boulet, P.; Greenwell, H. C.; Stackhouse, S.; Coveney, P. V. Recent advances in understanding the structure and reactivity of clays using electronic structure calculations. *J. Mol. Struct. (THEOCHEM)* **2005**, *762*, 33–48.

(2) Kloprogge, J. T. Synthesis of smectites and porous pillared clay catalysts: A Review. *J. Porous Mater.* **1998**, *5*, 5–41.

(3) Greenwell, H. C.; Jones, W.; Coveney, P. V.; Stackhouse, S. On the application of computer simulation techniques to anionic and cationic clays: A materials chemistry perspective. *J. Mater. Chem.* **2006**, *16*, 708–723.

(4) Almon, W. R.; Johns, W. D. Petroleum forming reactions: the mechanism and rate of clay catalyzed fatty acid decarboxilation. *Adv. Org. Geochem., Proc. Int. Meet. 7th* **1975**, *7*, 157–171.

(5) Geatches, D. L.; Clark, S. J.; Greenwell, H. C. Role of clay minerals in oil-forming reactions. *J. Phys. Chem. A* **2010**, *114*, 3569–3575.

(6) Prat-Resina, X.; González-Lafont, A.; Lluch, J. M. How important is the refinement of transition state structures in enzymatic reactions? *J. Mol. Struct. (THEOCHEM)* **2003**, *632*, 297–307.

(7) Gao, J.; Truhlar, D. Quantum mechanical methods for enzyme kinetics. *Annu. Rev. Phys. Chem.* **2002**, *53*, 467–507.

(8) Raab, M.; Kozmon, S.; Tvaroska, I. Potential transition-state analogs for glycosyltransferases. Design and DFT calculations of conformational behavior. *Carbohydr. Res.* **2005**, *340*, 1051–1057.

(9) Ali, M. A.; Rajakumar, B. Rate coefficients for the reaction of OH with $CF_3CH_2CH_3$ (HFC-263fb) between 200 and 400 K: Ab Initio, DFT, and transition state theory calculations. *J. Comput. Chem.* **2010**, *31*, 500–509.

(10) Simons, J.; Jørgensen, P.; Taylor, H.; Ozment, J. Walking on Potential Energy Surfaces. *J. Phys. Chem.* **1983**, *87*, 2745–2753.

(11) Elber, R; Karplus, M. A method for determining reaction paths in large molecules - application to myoglobin. *Chem. Phys. Lett.* **1987**, *139*, 375–380.

(12) E, W. N.; Ren, W. Q.; Vanden-Eijnden, E. String method for the study of rare events. *Phys. Rev. B* **2002**, *66*, 052301–4.

(13) Dellago, C.; Bolhuis, P. G.; Csajka, F. S.; Chandler, D. Transition path sampling and the calculation of rate constants. *J. Chem. Phys.* **1997**, *108*, 1964–1977.

(14) Koslover, E. S.; Wales, D. J. Comparison of double-ended transition state search methods. *J. Chem. Phys.* **2007**, *127*, 134102–12.

(15) Sinclair, J. E.; Fletcher, R. A new method of saddle-point location for the calculation of defect migration energies. *J. Phys. C: Solid State Phys.* **1974**, *7*, 864–870.

(16) Pokidova, T. S.; Denisov, E. T.; Shestakov, A. F. Kinetic parameters and geometry of the transition state of decarboxylation reactions of carboxyl and formyl radicals. *Pet. Chem.* **2008**, *48*, 174–185.

(17) Kakkar, R.; Pathak, M.; Radhika, N. P. A DFT study of the structures of pyruvic acid isomers and their decarboxylation. *Org. Biomol. Chem.* **2006**, *4*, 886–895.

(18) Li, J.; Brill, T. B. Spectroscopy of hydrothermal reactions 20: experimental and DFT computational comparison of decarboxylation of dicarboxylic acids connected by single, double, and triple bonds. *J. Phys. Chem. A* **2002**, *106*, 9491–9498.

(19) Tietze, L. F.; Kinzel, T.; Schmatz, S. Determination of the origin of stereoselectivity in multiple-transition-state reactions using DFT calculations: enantioselective synthesis of homoallylic alcohols from aliphatic methyl ketones via an auxiliary-mediated allylation. *J. Am. Chem. Soc.* **2008**, *130*, 4386–4395.

(20) Yang, T.; Wen, X. D.; Li, J. F.; Yang, L. M. Theoretical and experimental investigations on the structures of purified clay and acid-activated clay. *Appl. Surf. Sci.* **2006**, *252* (18), 6154–6161.

(21) Meheut, M.; Lazzeri, M.; Balan, E.; Mauri, F. Equilibrium isotopic fractionation in the kaolinite, quartz, water system: Prediction from first-principles density-functional theory. *Geochim. Cosmochim. Acta* **2007**, *71*, 3170–3181.

(22) Rignanese, G. M.; Gonze, X.; Pasquarello, A. First-principles study of structural, electronic, dynamical, and dielectric properties of zircon. *Phys. Rev. B* **2001**, *63*, 1043051–1043057.

(23) Gonze, X.; Charlier, J.-C.; Allan, D. C.; Teter, M. P. Interatomic force constants from first principles: The case of α-quartz. *Phys. Rev. B* **1994**, *50*, 13035–13038.

(24) Greenwell, H. C.; Stackhouse, S.; Coveney, P. V.; Jones, W. A Density functional theory study of catalytic *trans*-esterification by *tert*-butoxide MgAl anionic clays. *J. Phys. Chem. B* **2003**, *107*, 3476–3485.

(25) Breger, I. A. Diagenesis of metabolites and a discussion of the origin of petroleum hydrocarbons. *Geochim. Cosmochim. Acta* **1960**, *19*, 297–308.

(26) Kalnes, T.; Marker, T.; Shonnard, D. R. Green diesel: A second generation biofuel. *Int. J. Chem. React. Eng.* **2007**, *5*, A48.

(27) Wyckoff, R. W. G. *Crystal Structures*; John Wiley and Sons: Chichester, 1968.

(28) Larentzos, J. P.; Greathouse, J. A.; Cygan, R. T. An ab initio and classical molecular dynamics investigation of the structural and vibrational properties of talc and pyrophillite. *J. Phys. Chem. C* **2007**, *111* (34), 12752–12759.

(29) Clark, S. J.; Segall, M. D.; Pickard, C. J.; Hasnip, P. J.; Probert, M. J.; Refson, K.; Payne, M. C. *Z. Kristallogr.* **2005**, *220* (5), 567–570.

(30) Kohn, W.; Sham, L. J. Self-consistent equations including exchange and correlation effects. *Phys. Rev.* **1965**, *140* (4A), A1133–A1138.

(31) Kohn, W.; Sham, L. J. Quantum density oscillations in an inhomogeneous electron gas. *J. Phys. Rev.* **1965**, *137* (6A), A1697–A1705.

(32) Perdew, J. P.; Burke, K.; Ernzerhof, M. Generalized gradient approximation made simple. *Phys. Rev. Lett.* **1996**, *77* (18), 3865–3868.

(33) Kurth, S.; Perdew, J. P.; Blaha, P. Molecular and solid state tests of density functional approximations: LSD, GGAs, and meta-GGAs. *Int. J. Quantum Chem.* **1999**, *75*, 889–909.

(34) Vanderbilt, D. Soft self-consistent pseudopotentials in a generalized eigenvalue formalism. *Phys. Rev. B* **1990**, *41* (11), 7892–7895.

(35) Mazari, N.; Vanderbilt, D.; Payne, M. C. Ensemble density functional theory for *ab initio* molecular dynamics of metals and finite-temperature insulators. *Phys. Rev. Lett.* **1997**, *79* (7), 1337–1340.

(36) Govind, N.; Petersen, M.; Fitzgerald, G.; King-Smith, D.; Andzelm, J. A generalized synchronous transit method for transition state location. *Comput. Mater. Sci.* **2003**, *28*, 250–258.

(37) Gonze, X. First-principles responses of solids to atomic displacements and homogeneous electric fields: Implementation of a conjugate-gradient algorithm. *Phys. Rev. B* **1997**, *55*, 10337–10354.

(38) Lin, J. S.; Qteish, A.; Payne, M. C.; Heine, V. Optimized and transfereable nonlocal separable *ab initio* pseudopotentials. *Phys. Rev. B* **1993**, *47*, 4174–4180.

(39) Teter, M. P.; Payne, M. C.; Allan, D. C. Solution of Schrödinger's equation for large systems. *Phys. Rev. B* **1989**, *40*, 12255–12263.

(40) Zhang, A.; Ma, Q.; Wang, K.; Tang, Y.; Goddard, W. A. Improved processes to remove naphthenic acids. Final Technical Report DE-FC26−02NT15383, California Institute of Technology, 1200 East California Blvd., Pasadena, CA 91125, 2005.

(41) Senol, O.; Viljava, T. R.; Krause, A. O. I. Hydrodeoxygenation of methyl esters on sulphided NiMo/γ-Al_2O_3 and CoMo/γ-Al_2O_3 catalysts. *Catal. Today* **2005**, *100*, 331–335.

(42) Fukui, K. The path of chemical reactions - the IRC approach. *Acc. Chem. Res.* **1981**, *14*, 363–368.

(43) Kraka, E.; Cremer, D. Computational analysis of the mechanism of chemical reactions in terms of reaction phases: Hidden intermediates and hidden transition states. *Acc. Chem. Res.* **2010**, *43*, 591–601.

(44) Farmer, V. C. *The Infrared Spectra of Minerals*; Mineralogical Society: London, 1974.

(45) Sainz-Diaz, C. L.; Escamilla-Roa, E.; Hernandez-Laguna, A. Pyrophyllite dehydroxylation process by first principles calculations. *Am. Mineral.* **2004**, *89*, 1092–1100.

(46) Mulliken, R. S. Electronic population analysis on LCAO-MO molecular wavefunctions * 1. *J. Chem. Phys.* **1955**, *23* (10), 1833–1840.

(47) Suter, J. L.; Anderson, R. L.; Greenwell, H. C.; Coveney, P. V. Recent advances in large-scale atomistic and coarse-grained molecular dynamics simulation of clay minerals. *J. Mater. Chem* **2009**, *19*, 2482–2493.

(48) Smith, B.; Greenwell, H. C.; Whiting, A. Catalytic upgrading of tri-glycerides and fatty acids to transport biofuels. *Energy Environ. Sci.* **2009**, *2*, 262–271.